Biological and Medical Applications of Materials and Interfaces

O2-Cu/ZIF-8@Ce6/ZIF-8@F127 Composite as a Tumor Microenvironment-Responsive Nanoplatform with Enhanced Photo/Chemo-Dynamic Antitumor Efficacy

Zhongxi Xie, Shuang Liang, Xuechao Cai, Binbin Ding, Shanshan Huang, Zhiyao Hou, Ping'an Ma, Ziyong Cheng, and Jun Lin

ACS Appl. Mater. Interfaces, **Just Accepted Manuscript** • DOI: 10.1021/acsami.9b10685 • Publication Date (Web): 09 Aug 2019

O_2-Cu/ZIF-8@Ce6/ZIF-8@F127 Composite as a Tumor Microenvironment-Responsive Nanoplatform with Enhanced Photo/Chemo-Dynamic Antitumor Efficacy

Zhongxi Xie, ‡, § Shuang Liang,‡, §, Xuechao Cai,§ Binbin Ding,‡, § , Shanshan Huang, ‡ Zhiyao Hou, ‡ Ping ′an Ma, ‡ Ziyong Cheng*‡, § and Jun Lin* ‡, §

‡ State Key Laboratory of Rare Earth Resource Utilization, Changchun Institute of Applied Chemistry, Chinese Academy of Sciences, Changchun 130022, PR China.

§ University of Science and Technology of China, No. 96, JinZhai Road, Baohe District, Hefei, Anhui 230026, P. R. China.

KEYWORDS: photodynamic therapy; chemodynamic therapy; metal-organic frameworks; hypoxia; oxygen delivery; glutathione.

ABSTRACT: Hypoxia and overexpression of glutathione (GSH) are typical characteristics of the tumor microenvironment (TME), which severely hinders cancer treatments. Here we design a novel biodegradable therapeutic system, O_2-Cu/ZIF-8@Ce6/ZIF-8@F127 (OCZCF), to simultaneously achieve GSH depletion and O_2-enhanced combination therapy. Notably, the doped Cu^{2+} doubles the O_2 storage capacity of ZIF-8 matrix, which makes OCZCF an excellently pH-sensitive O_2 reservoir for conquering tumor hypoxia, enhancing the photodynamic therapy (PDT) efficiency of Ce6 under 650 nm laser irradiation. Moreover, the released Cu^{2+} can act as a smart reactive oxygen species (ROS) protector by consuming intracellular GSH. The byproduct Cu^{+} will undergo highly efficient Fenton-like reaction to achieve chemodynamic therapy (CDT) in the presence of abundant H_2O_2. The accompanying O_2

will further alleviate hypoxia. The in vitro and in vivo experimental data indicate that OCZCF could cause remarkable tumor inhibition through enhanced synergetic PDT and CDT, which may open up a new path for cancer therapy.

1. INTRODUCTION

The recent report suggests that cancer death rates have decreased over the past two decades. However, malignant tumors are still one of the diseases that currently pose a serious threat to human health and life. Hence, fighting against tumors needs continued basic and clinical research.[1] Nowadays, photodynamic therapy (PDT) and chemodynamic therapy (CDT) have emerged as burgeoning cancer treatments.[2-9] For the most common type II PDT process, a photosensitizer (PS) is prerequisite to generate singlet oxygen ($^1O_2$) with the assistance of O_2 under a specific wavelength of light, then the $^1O_2$ will induce cell apoptosis.[2-5] CDT is first proposed by Bu and Shi et al., iron-based Fenton reaction is primitively utilized to kill cancer cells via transforming intracellular H_2O_2 to the highly cytotoxic hydroxyl radicals (•OH).[6] Afterwards, MnO_2 and copper ions are also developed for CDT.[7-9] Exactly, the $^1O_2$ and •OH are the most widespread components in reactive oxygen species (ROS), which can cause great damages to tumor cells. Besides, the literature has shown that ROS-mediated cancer treatment may cause more damages to cancer cells than normal cells due to the different redox states, making them extremely competitive in the treatment of cancers.[10]

However, the tumor microenvironment (TME) with hypoxia seriously affects the therapeutic efficiency.[11,12] Type II PDT mechanism involves the change from triplet ground state molecular oxygen ($^3O_2$) to the more reactive $^1O_2$. So this process requires the participation of O_2 and will result in a large amount of O_2 consumption.[11,12] Unfortunately, the rapid proliferation of tumors lead to the widespread hypoxia in solid tumors.[13] Thus, the PDT process will in turn aggravate hypoxia. Such a vicious cycle would greatly reduce the effectiveness of PDT. To solve this problem, some O_2 storage materials, such as hemoglobin,[14,15] perfluorocarbon[16,17] and metal-organic frameworks (MOFs),[18-20] have been employed to relieve the hypoxia within tumors. In addition, some nanozymes are also widely utilized for in situ O_2 generation to relievie intracellular hypoxia, mainly including catalase,[21,22] MnO_2,[23,24] platinum(IV) diazido complexes,[25] platinum,[26] $MnFe_2O_4$,[27] carbon nitride[28] and so on.

Another challenge for cancer therapy is that glutathione (GSH) is inherently excessive in tumor sites (up to 10 mM).[29,30] The strong reducibility of GSH consumes cytotoxic ROS produced by therapeutic agents, which would significantly reduce the efficiency of cancer treatment. Therefore, reducing intracellular GSH is very necessary for

oncotherapy. At present, the most common method is using nanomaterials to reduce intracellular GSH levels. For instance, Stone and coworkers employed a cysteinase enzyme to reduce L-cysteine, which is essential for the production of GSH, thereby decreasing the level of intracellular GSH indirectly.[31] Tan's group and Chen's group reported MnO_2 nanosystems for enhanced cancer therapy by reducing endocellular GSH content, respectively.[8,32] Qu's group employed copper(II)-graphitic carbon nitride to improve ROS accumulation and reduce GSH content for enhanced PDT.[33]

In fact, the complicated TME can make tumors drug resistant, limiting single cancer therapies. Combination therapy can solve this problem well, which presents a promising strategy for oncotherapy. The most marvelous advantage of this program is that it can minimize the drug doses while maximizing its efficacy.[34-36] Therefore, exploring novel system that could integrate multiple treatments is of great significance.

Metal-organic frameworks (MOFs) are porous organic-inorganic hybrid materials assembled by organic ligands and metal ions via coordinate bonds.[37] Due to their unique advantages, such as porosity, variety of species, and degradability, making them biologically friendly and have been broadly studied for oncotherapy.[38-40] Some copper-

based MOFs, such as UMCM-152, HKUST-1, and NU-125, have been reported as excellent O_2 storage matrials attributed to coordinatively unsaturated Cu sites,[41,42] which shows great prospects in overcoming tumor hypoxia for enhanced PDT. Cu^{2+} can also play a role in reducing GSH.[33] Besides, a recent report reveals that copper-based materials could act as Fenton reagents for CDT.[9] However, The instability in vivo limits the biological applications of these Cu-based MOFs. Among MOFs family, zeolitic imidazolate frameworks (ZIFs) are first reported by Yaghi's group, which has exceptional chemical and thermal stability.[43] Our group recently reported the use of ZIF-90 as an O_2 carrier to overcome tumor hypoxia for enhanced PDT.[18] However, due to the innate limitation of ZIF materials, its oxygen storage capacity is confined. ZIF-8 is an another classic material belonging to ZIFs. Interestingly, ZIF-8 is degradable in acid TME. Moreover, the preparation condition of ZIF-8 is mild and the cost is relatively low, so ZIF-8 has been broadly utilized as a pH-degradable drug carrier in nanomedicine.[21,44,45] It has been reported that ZIF-8 possesses the ability to store O_2.[46] Nevertheless, it is still limited compared with those copper-containing MOFs.[41,42] In view of this, we speculate that by doping Cu^{2+} into ZIF-8, the O_2 storage capacity can be

enhanced. On this basis, if the PS is further integrated into it, a therapeutic platform with enhanced PDT and CDT could be obtained, which would show great potential for TME-responsive combination therapy.

As a proof-of-concept study, the O_2-Cu/ZIF-8@Ce6/ZIF-8@F127 (OCZCF) core-shell nanostructure is designed to simultaneously overcome tumor hypoxia and reduce GSH level for enhanced PDT and CDT. As shown in **Scheme 1**, Cu^{2+}-doped ZIF-8 (Cu/ZIF-8) is first fabricated via a simply ion doping stratagy. Then, a thin layer of ZIF-8 encapsulating the well-known PS, i.e. Ce6, is coated on Cu/ZIF-8, followed by overlaying a layer of F127, which is a highly biocompatible polymer. After intravenous (i.v.) injection, OCZCF could accumulate in

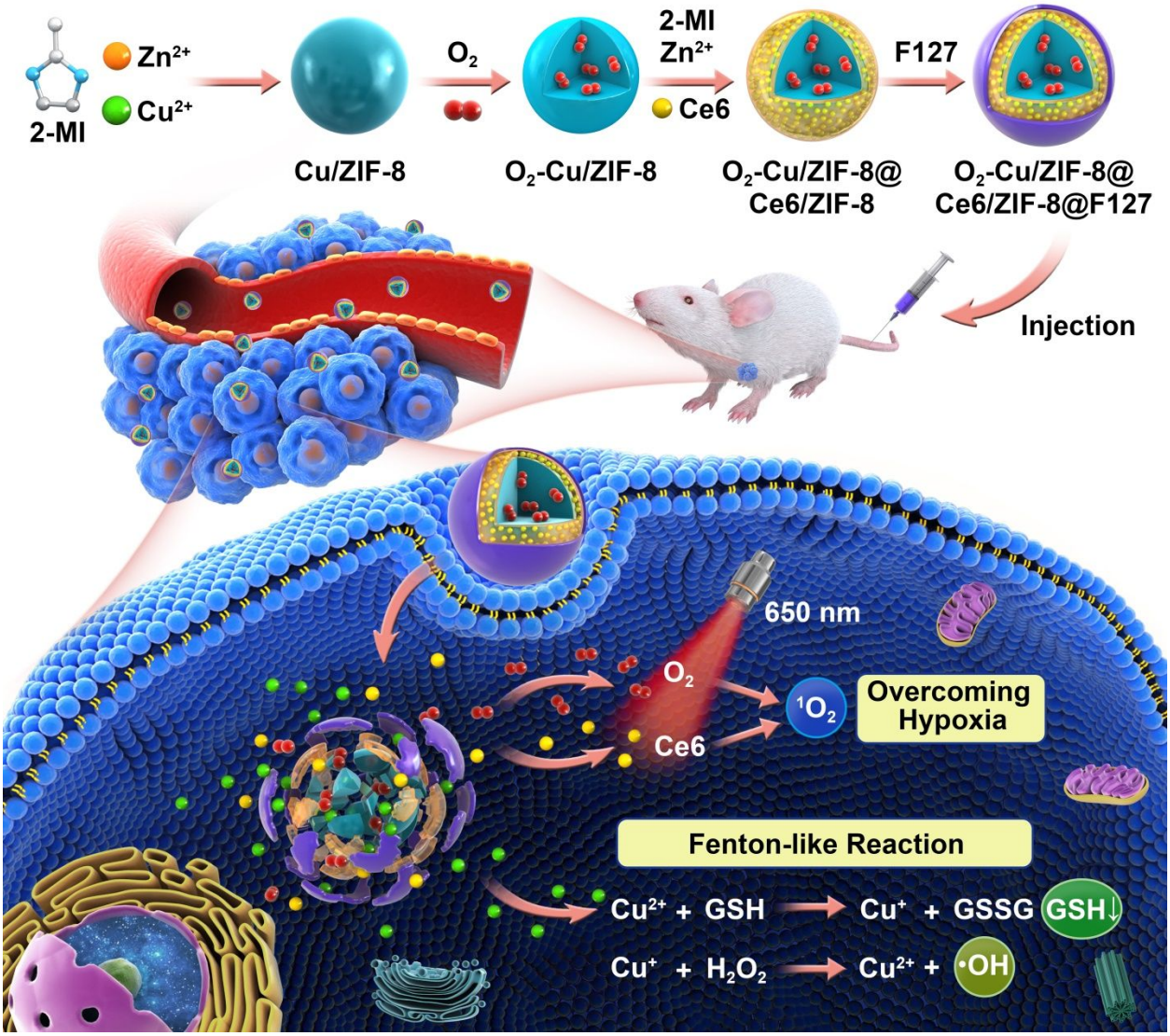

Scheme 1. The schematic illustration of the fabrication process of tumor microenvironment- responsive OCZCF nanoplatform for enhanced PDT and CDT through GSH depletion and O_2 replenishment.

tumor site due to the enhanced permeability and retention (EPR) effect,[47-49] resulting in the release of O_2, Ce6, and Cu^{2+} in the mild acidic TME. The large amount of O_2 would alleviate tumor hypoxia and allow the quick generation of abundant cytotoxic $^1O_2$ by Ce6 under 650 nm laser irradiation. In addition, the released Cu^{2+} could oxidize intratumoral GSH, inducing GSH depletion. The generated Cu^+ could futher react with H_2O_2 in TME, inducing high efficient Fenton-like reaction to generate •OH and O_2 for CDT. As a result, this integrated nanodrug shows synergistically enhanced antitumor efficacy both in vitro and in vivo.

2. RESULTS AND DISCUSSION

2.1. Fabrication of O_2-Cu/ZIF@Ce6/ZIF-8@F127 Nanocomposites (OCZCF). Cu/ZIF-8 crystals doped with different amount of Cu ions were fabricated via a simple ion doping stratagy modified from the literature.[50,51] The particle size and yield were evaluated using dynamic light

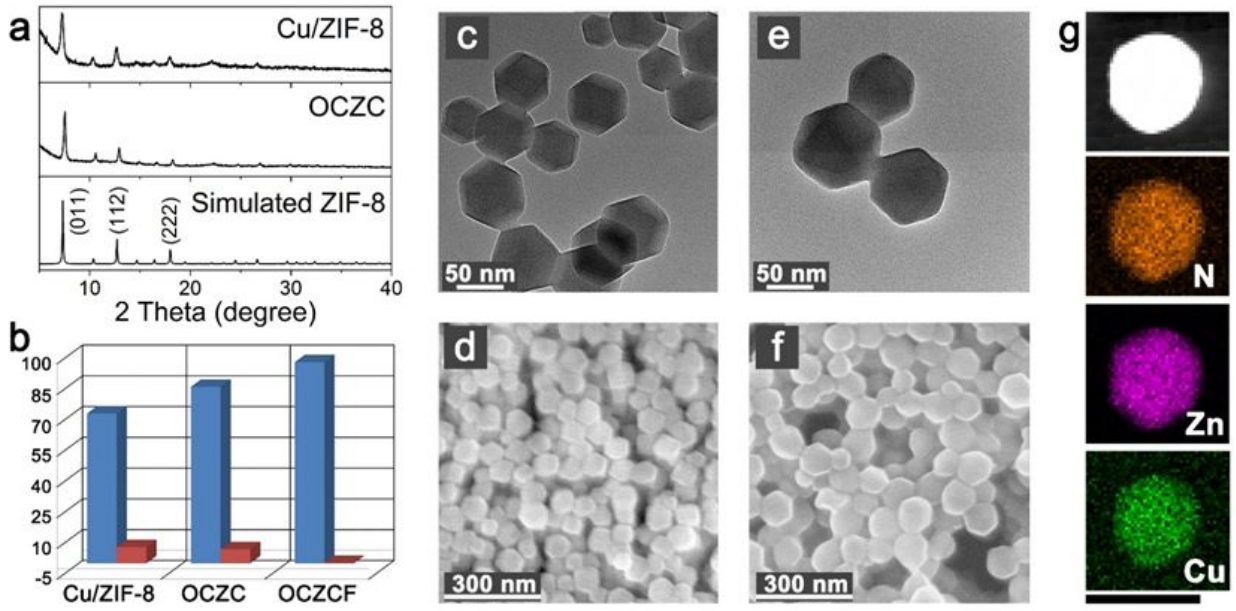

Figure 1. (a) PXRD patterns of Cu/ZIF-8 and OCZC compared with simulated ZIF-8 pattern. (b) DLS and surface potential analysis of Cu/ZIF-8, OCZC, and OCZCF, respectively. Blue bars indicate the particle size (nm). Red bars are Zeta potential (mV). TEM images of (c) Cu/ZIF-8 and (e) OCZCF. SEM images of (d) Cu/ZIF-8 and (f) OCZCF. (g) HAADF-STEM images of OCZC. The scale bar represents 100 nm.

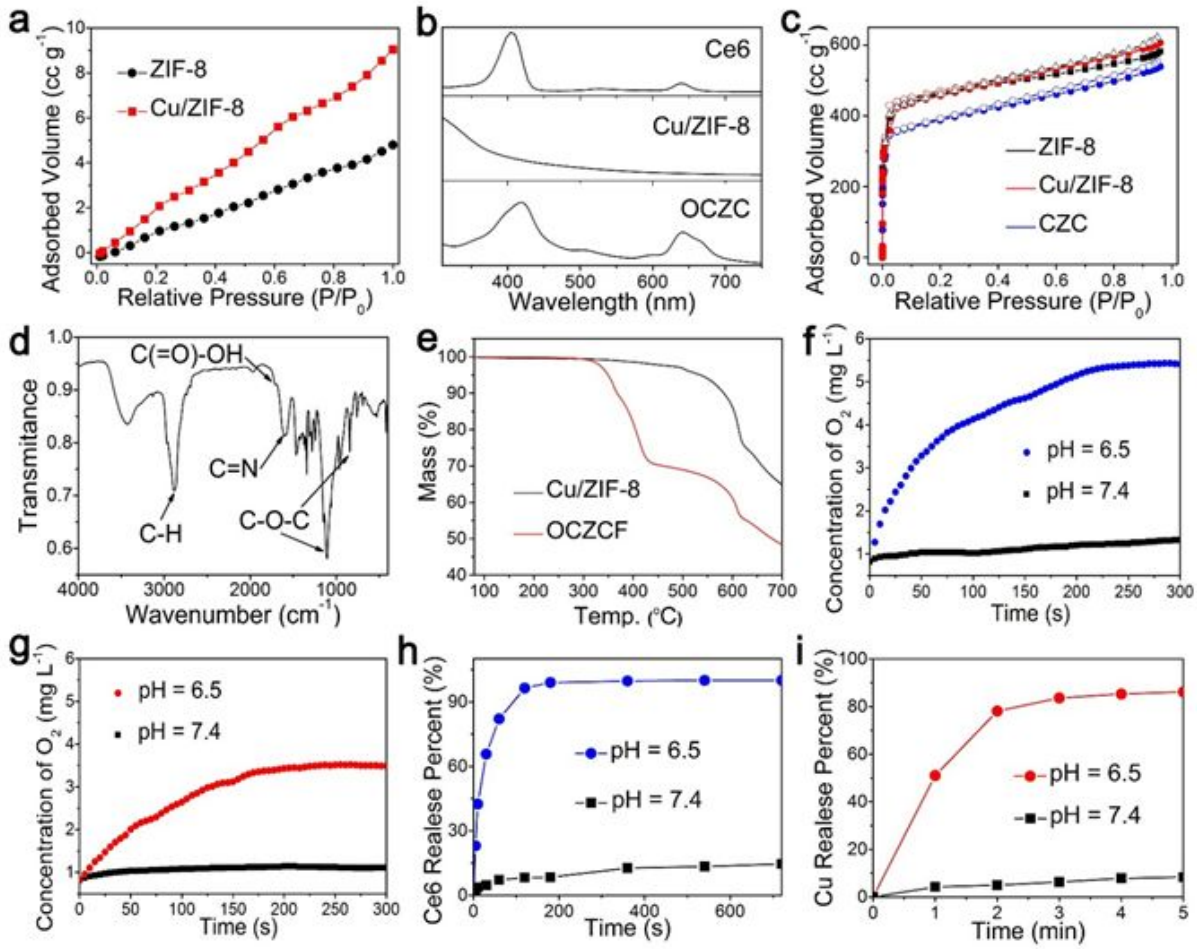

Figure 2. (a) O_2 adsorption isotherm of ZIF-8 and Cu/ZIF-8 crystal. (b) UV-vis absorption spectra of Ce6, Cu/ZIF-8, and OCZC. (c) N_2 adsorption (solid symbols)/desorption (hollow symbols) isotherms of ZIF-8, Cu/ZIF-8, and CZC. (d) FT-IR spectra of OCZCF. (e) TGA curves of Cu/ZIF-8 and OCZCF. O_2 release behavior of (f) OCZCF and (g) O_2-ZIF-8. (h) Ce6 release behavior of OCZCF. (i) Cu released behavior of OCZCF after soaking in PBS solutions for different time point.

scattering (DLS) and inductively coupled plasma (ICP) analysis (**Figure S1 and Table S1**). As the Cu^{2+} content increasing, the crystal size increases dramatically while the product yield decreases fast. Powder X-ray diffraction (PXRD) indicates that the doped Cu^{2+} does not affect the crystal structure of ZIF-8 (**Figure 1a and Figure S2**). It is reported that nano carriers in the sub-100 nm size could be transported into tumor blood vessels via EPR effect.[47-49] Therefore, we optimize the feeding ratio of Cu^{2+} to be 25%. DLS analysis, transmission electron microscope (TEM) and scanning electron microscope (SEM) pictures show the size of Cu/ZIF-8 is about 75 nm (**Figure 1b-d and Table S2**). The O_2 adsorption isotherms confirm the enhanced O_2 storage capacity of Cu/ZIF-8. At 1 atmospheric pressure, the adsorbed O_2 volume of Cu/ZIF-8 is about twice higher than pure ZIF-8 (**Figure 2a**). Meanwhile, it is up to 6.7 times higher than hemoglobin, which is the normal oxygen storage component of human body with the maximun O_2-binding capacity of 1.34 cc g^{-1}.[52,53] This result implies that Cu/ZIF-8 could act as a more effective oxygen carrier than hemoglobin.

After loading O_2, ZIF-8 shell grows spontaneously onto the Cu/ZIF-8 seed attributed to the isotropy.[54] Ce6 is embedded into ZIF-8 shell by a one-pot process at the same time.[55] The O_2-Cu/ZIF-8@Ce6/ZIF-8 (OCZC) with an average size of 85 nm is obtained. (**Figure 1g** and **Table S2**). EDS mapping results (**Figure 1g**) testify the uniformly dispersed cuprum in Cu/ZIF-8 core, further confirming the core-shell structure. The loading amount of Ce6 is calculated to be 3.34 wt% by UV-vis absorption spectra (**Figure 2b and Figure S3**). Nitrogen adsorption/desorption experiments show the type I isotherms of Cu/ZIF-8 and CZC, suggesting the presence of micropores (**Figure 2c and Table S3**). Finally, an amphiphilic polymer Pluronic F127, approved by the US Food and Drug Administration, was coated around OCZC to improve the biocompatibility of nanocomposites.[56-57] DLS, TEM and SEM results show the size of O_2-Cu/ZIF-8@Ce6/ZIF-8@F127 (OCZCF) increased to about 95 nm (**Figure 1b, 1e, 1f, and Table S2**). The doped Cu^{2+} sites were also determined via X-ray photoelectron spectroscopy (XPS). The peaks at 934.1 and 953.8 eV are assigned to the Cu($2p_{3/2}$) and Cu($2p_{1/2}$) of Cu^{2+}, respectively[58,59] (**Figure S4**). The satellite peak at around 942.3 eV also indicates the characteristic of Cu^{2+}. In Fourier transform infrared (FT-IR) spectra, the absorption

peaks at 1584 and 1710 cm^{-1} are the C=N and C(=O)-OH stretching vibration in ZIF-8[60] and Ce6[61], respectively (**Figure 2d**). Peaks at 2873, 1100 and 840 cm^{-1} belong to the vibration of C-H and C-O-C bonds in F127[62]. Thermogravimetric analyses (TGA) show an additional sharp weight loss of OCZCF between 300 to 450 °C compared with Cu/ZIF-8, corresponding to the decomposition of Ce6[63] and F127[64] (**Figure 2e**).

2.2. pH-Responsive Drug Release Behavior. To characterize the pH-degradability of OCZCF, nanoparticles were soaked in PBS buffer with pH = 7.4 and 6.5, respectively. The SEM and TEM images of the precipitation were shown in **Figure S5** and **S6**. In neutral environment (pH = 7.4), the crystal keeps its morphorlogy. However, when treated with acidic PBS solution, the crystal structure rapidly disassembles over time. The complete collapse of OCZCF could be observed after 10 min stirring, confirming the pH-sensitiveness of OCZCF.[44]

In addition, the O_2 release behavior of OCZCF in deoxidized PBS buffer is shown in **Figure 2f**. In acidic condition (pH = 6.5), the curve increases sharply whereas only a plateau is observed in the neutral counterpart, indicating the pH-responsive O_2 release

property. Moreover, compared with O_2-ZIF-8 (**Figure 2g**), the amount of O_2 released by OCZCF increases by 1.7 times, which reveals the expanded O_2 loading capacity after doping with Cu ions. Furthermore, the released Ce6 and Cu^{2+} were detected via UV-Vis spectroscopy and ICP, respectively (**Figure 2h, 2i and Table S4**). As the pH value decreases to 6.5, more than 90% of Ce6 and 85% of Cu^{2+} are released due to the decomposition of OCZCF. The above results suggest that OCZCF has big potential to be used as an effective on-demand drug delivery system.

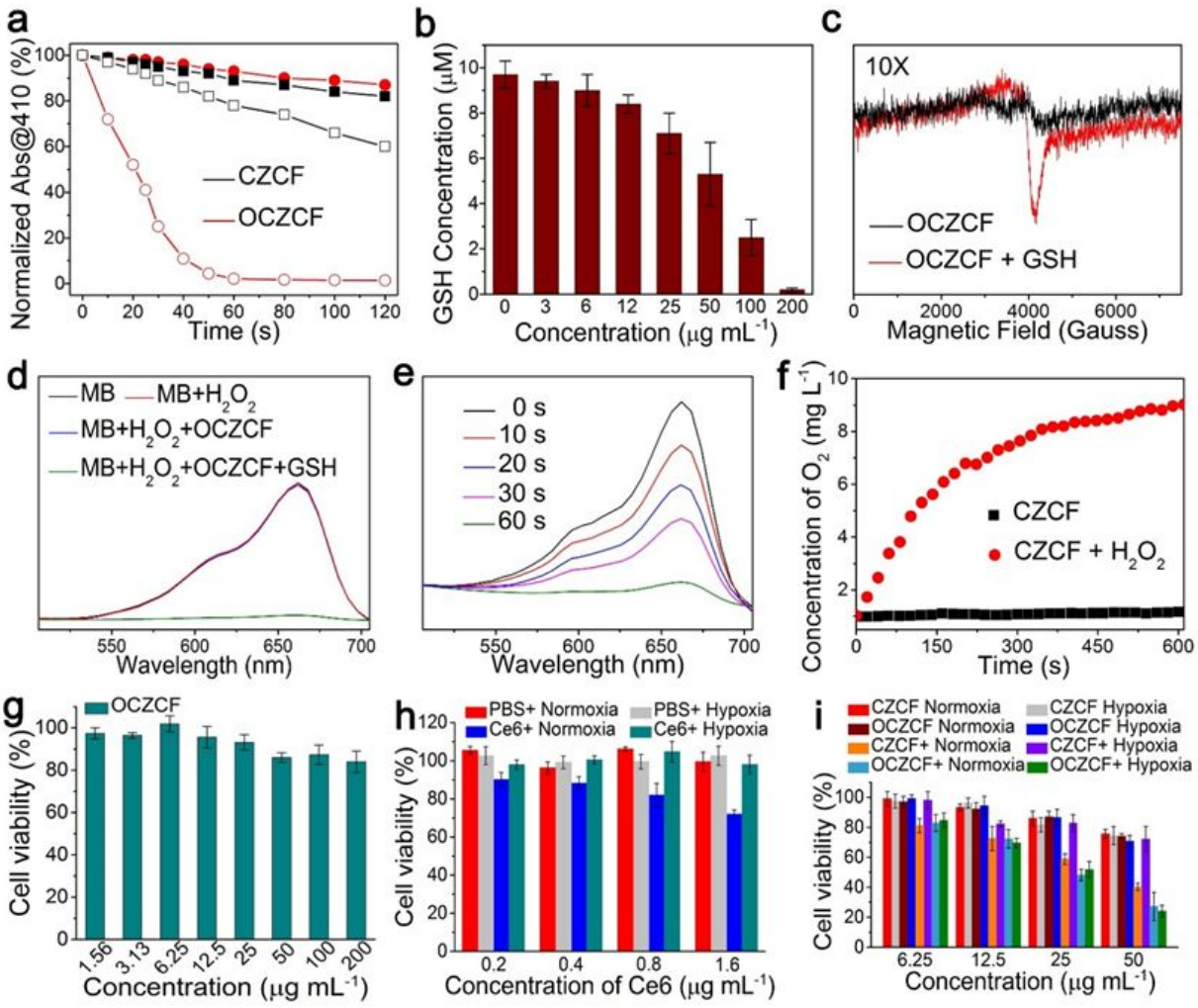

Figure 3. (a) ROS generation ability of CZCF and OCZCF in deoxidized PBS buffer (pH = 7.4 (solid symbols) and 6.5 (hollow symbols)) assessed by DPBF. (b) GSH concentration after treating with different amount of OCZCF in PBS buffer (pH = 6.5) for 10 min. (c) ESR spectra of OCZCF before and after the addition of GSH. (d) MB adsorption spectra in different mixture with pH = 6.5. (e) The degradation process of MB after incubation with the mixture of H_2O_2, OCZCF, and GSH for 1, 10, 20, 30, or 60 s. (f)

Dissolved O_2 concentration in CZCF solution (pH = 6.5) before and after the addition of H_2O_2. (g) Relative viabilities of L929 cells after incubation with different concentrations of OCZCF in the absence of light irradiation for 24 h. (h) Relative viabilities of PBS+ or Ce6+ treated 4T1 cells in normoxic or hypoxic environment. (i) Relative viability of 4T1 cells incubated with different composites in normoxic or hypoxic environment. Error bars indicate the standard deviations (n = 6).

2.3. ROS Detection and GSH Consumption. It was reported that 1,3-diphenylisobenzofuran (DPBF) could undergo a Diels-Alder 1,4-cycloaddition reaction with $^1O_2$, inducing the decrease of its absorption at 410 nm.[22, 44] Therefore, we used DPBF to characterize the production of $^1O_2$ of different composites under 650 nm light irradiation. As shown in **Figure 3a,** the degradation rate of DPBF in neutral solution is much lower than that in acidic condition. This could be explained by the reduced photo-quenching effect of Ce6 after the decomposition of nanocomposites in acidic condition.[45] Interestingly, the most significant decrease is observed for DPBF treated with OCZCF in acidic solution, revealing that the released O_2 could greatly enhance the

$^1O_2$ generation ability of Ce6 in hypoxic environment. Moreover, electron spin resonance (ESR) measurements were carried out to identify the generated $^1O_2$, and 2,2,6,6-tetramethylpiperidine (TEMP) was used as the trapping agent to detect $^1O_2$ generation. As shown in **Figure S7**, the ESR spectrum of OCZCF upon light shows a 1:1:1 triplet signal, which belongs to 2,2,6,6-tetramethylpiperidine-N-oxyl (TEMPO)[65]. This result directly confirms the generation of $^1O_2$.

Besides, the Cu^{2+}-involved GSH consumption was validated using a reduced GSH assay kit.[46] Compared with the control group and ZIF-8 treated solution, the concentration of GSH decreased obviously when treated with Cu/ZIF-8 (**Figure S8**). Moreover, the GSH concentration exhibits a dose-dependent manner with the amount of OCZCF (**Figure 3b**), indicating the GSH depletion by OCZCF. Meanwhile, the byproduct, Cu^+, was confirmed via XPS and ESR spectroscopy in term of the disappearence of the satellite peak in XPS and the intense signal in the high field of Cu^{2+} in ESR spectrum, respectively (**Figure 3c and Figure S9**).[9,51]

The generated cuprous ions were reported to be more active in producing •OH in mild acidic TME (pH = 6.5) than the traditionally used Fe^{2+} ions,[9] which shows big potential

for effecient CDT. Herein, ESR measurements were performed to identify the generation of •OH, and 5,5-dimethyl-1-pyrroline-N-oxide (DMPO) was used as the trapping agent. As shown in **Figure S10**, the ESR spectrum of OCZCF with H_2O_2 shows a 1:2:2:1 quartet characteristic with the addition of DMPO due to the generation of DMPO-OH, demonstrating •OH formation by OCZCF.[65] Then, methyl blue (MB) was employed further for •OH detection. When treated with H_2O_2 or H_2O_2+OCZCF, the absorption peak intensity of MB almost does not change in comparision with pure MB solution (**Figure 3d**). However, it decreases sharply in the coexistence of MB, H_2O_2, GSH and OCZCF, which reveals the generation of •OH. Besides, **Figure 3e** shows the time-dependent degradation process of MB in the mixture of MB, H_2O_2, GSH and OCZCF, suggesting the GSH-assisted Fenton-like reaction of OCZCF. Furthermore, the dissolved oxygen meter demonstrates that CZCF could successfully catalyze H_2O_2 to generate O_2, which provides the possibility for further alleviation of hypoxia owing to the high H_2O_2 concentration of TME (**Figure 3f**).

2.4. Cell Apoptosis Analysis. Before cytotoxic assay, the biocompatibility of OCZCF on L929 cells was assessed via 3-(4,5- dimethylthiazol-2)-2,5-diphenyltetrazole bromide

(MTT) assay. As shown in **Figure 3g**, cells treated with different amount of OCZCF show high survival rate even at a concentration of 200 μg mL^{-1}, indicating the biostability of OCZCF. Cellular uptake mechanism was investigated by ICP. As shown in **Table S5**, due to its good biocompatibility, the OCZCF can be endocytosed gradually by L929 (mouse fibroblast cells) and 4T1 cells (mouse breast cancer cells) at 6 h.

Figure S11 shows the GSH content of 4T1 cells incubated with PBS (control group), ZCF (ZIF-8@Ce6/ZIF-8@F127) and CZCF, respectively. For cells treated with different amount of ZCF, the GSH concentration stays in relatively high level compred with the control group. Whereas for CZCF treated group, the amount of intracellular GSH drops quickly as the drug concentration increasing. These data reveal that the copper-containing CZCF composites are able to consume GSH in tumor cells, which brings the possibility for high efficient PDT and CDT.

Next, in vitro therapeutic effect was characterized by MTT assay on 4T1 cells treated with PBS with light (PBS+), Ce6 with light (Ce6+), CZCF, OCZCF, CZCF+, and OCZCF+, respectively. Cells were exposed to normoxic (21 % oxygen) or hypoxic (1% oxygen) environments. As shown in **Figure 3h**, light irradiation at low power density

shows negligible effect towards 4T1 cells. For Ce6+ treated groups, the cell viability in hypoxia is much higher than that in normoxia, which suggests the cytotoxicity of Ce6 is greatly dependent on O_2 concentration. **Figure 3i** shows the curative effect of CZCF and OCZCF under normoxia and hypoxia, respectively. For cells treated with 21% O_2, the cellular lethality in all groups exhibits a dose-dependent manner, especially for light treated groups. This could be explained by the synergetic effect of CDT and PDT. However, the cell viability varies in hypoxic condition. In comparation with deoxidized counterparts, OCZCF shows significantly enhanced cytotoxicity, which proves the importance of hypoxia alleviation for synergetic therapy. Noted that the single treatment is less efficient, which reveals the advantage of synergetic therapy.

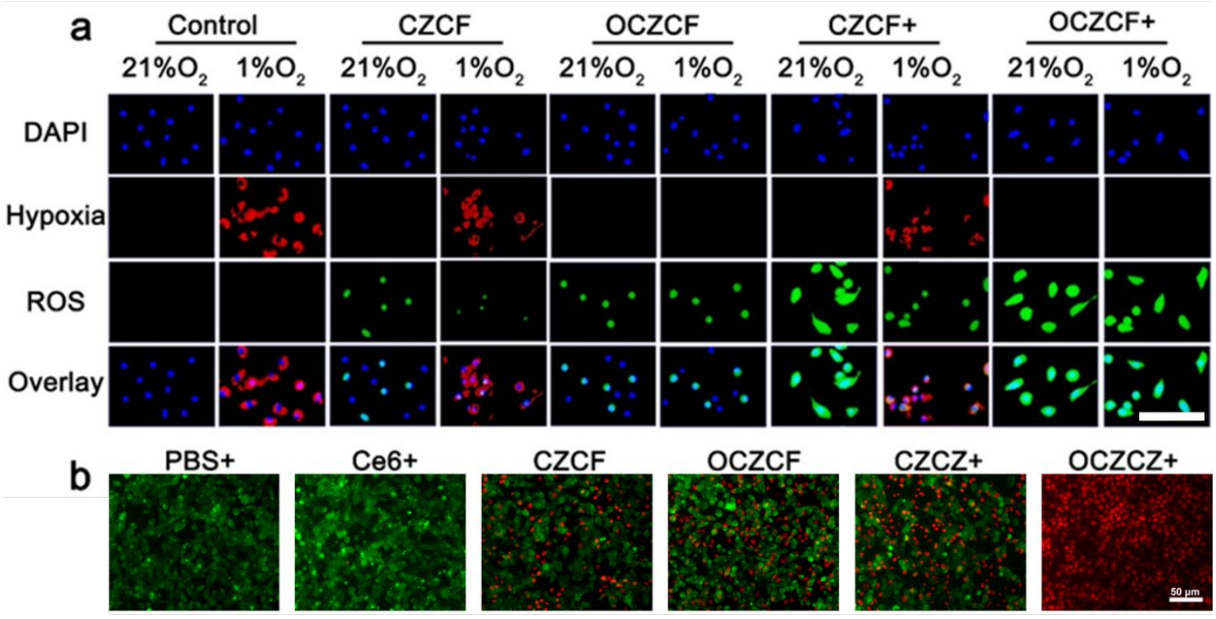

Figure 4. (a) In vitro ROS and hypoxia imaging of 4T1 cells. (b) Live/dead cell staining of 4T1 cells after incubation with PBS+, Ce6+, CZCF, OCZCF, CZCF+ or OCZCF+ under hypoxic condition. The green signals indicate the living cells. The red signals indicate the dead cells. Scale bar indicates 50 μm.

2.5. Intracellular Detection of ROS and Hypoxia. To evaluate the generation of O_2 and ROS in vitro, 4T1 cells were treated with PBS (noted as control group), CZCF, OCZCF, CZCF with light (CZCF+), or OCZCF with light (OCZCF+) under normoxia (21 % oxygen) or hypoxia (1% oxygen), respectively. The intracellular ROS and hypoxic condition were stained by a ROS/hypoxia detection kit (**Figure 4a**). Compared with the control group, the red signal decreases for CZCF and CZCF+ treated cells, which reveals the alleviation of hypoxia by Cu-mediated Fenton-like reaction. However, it is almost invisible in OCZCF and OCZCF+ treated groups due to the abundent O_2 released from OCZCF in acidic TME. The generated ROS through Fenton-like reaction is revealed by the green fluorecence appeared in CZCF and OCZCF treated cells, demonstrating the CDT process. Besides, after 650 nm light irradiation, the green signal sharply increases

both in CZCF+ and OCZCF+ treated groups. This could be explained by the enhanced ROS generation ability in the synergistic CDT and PDT. Most importantly, compared with CZCF and CZCF+, both OCZCF and OCZCF+ show enhanced ROS generation ability under hypoxic condition, respectively. These results indicate that the O_2-containing multifunctional OCZCF nanoplatform could successfully overcome tumor hypoxia and facilitate the generation of large amount of ROS in living tumor cells.

Furthermore, we also proved the effects by the immunofluorescence staining assay in vivo. It is well-known that the hypoxia in the TME can trigger the expression of hypoxia-inducible factor (HIF)-1α. To identify the nanoparticles possess the ability to relieve tumor hypoxia, mice tumor slices were obtained for HIF-1α (red) staining assay after being injected 24 h. Meanwhile, the production of ROS also has been demonstrated by tumor slices staining DCFH-DA (green) after different treatments (**Figure S12**). The results were consistent with those for in vitro experiments.

Besides, the in vitro cellular viability in hypoxia was also tested by a Live/Dead Cell Double Staining Kit. The red signal indicates dead cells while the green signal reveals living cell (**Figure 4b**). As expected, OCZCF+ show highest lethality, which is in

accordance with the MTT assay. Similar results are observed by flow cytometry analysis shown in **Figure S13**, which suggest that OCZCF nanodrug could be used for efficient tumor hypoxia alleviation and in vitro tumor therapy.

2.6. In Vivo Tumor Inhibition. 4T1-tumor bearing Balb/c mice were used for in vivo anti-tumor experiments. All mice were randomly divided into 6 groups for PBS, Ce6+, OCZCF, CZCF+, and OCZCF+ treatments, respectively. All drugs were tail intravenous injected into

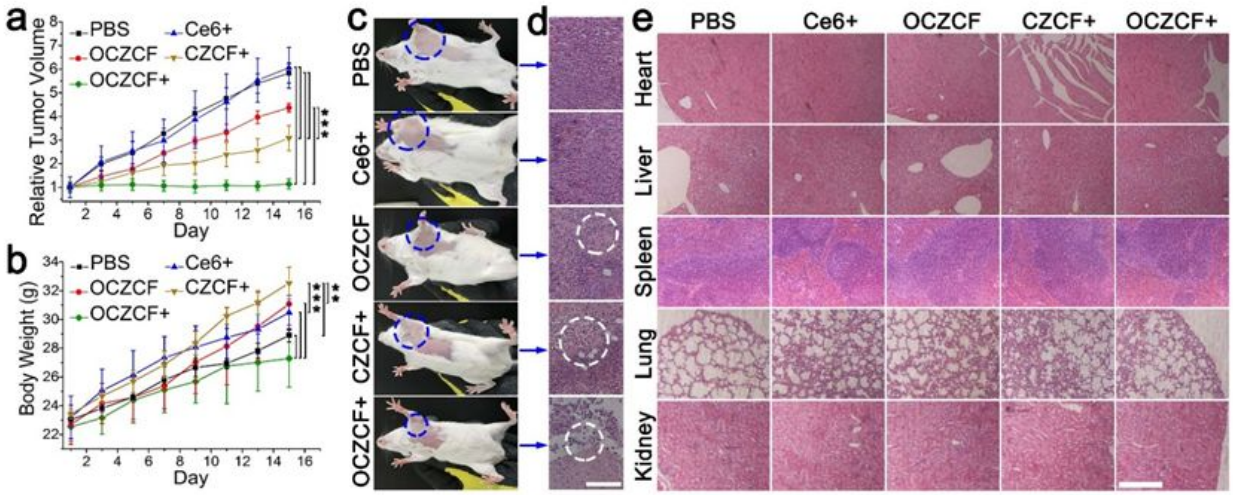

Figure 5 (a) Relative tumor volume and (b) average body weight of 4T1 tumor-bearing mice. Error bars indicate the standard deviations (n = 6). P values by comparing the CZCF+ or OCZCF+ group with other control groups were calculated by two-tailed

Student's t-test (***p < 0.001, **p < 0.01, or *p < 0.05) (c) Photos of mice at the end of treatments. Histological analysis of (d) tumor sections and (e) tissue sections at the end of treatments. Scale bars are 50 μm.

mice with the concentration of Ce6 to be 4.0 mg kg^{-1}. Then, the light treated (+) groups were exposed to 650 nm light for 10 min at the power dencity of 50 mW cm^{-2}. Tumor size and body weight of mice in each group were monitored for 15 days after drug treatment. As shown in **Figure 5a, 5c and Figure S14**, Ce6+ treated mice show similar tumor growth rate as PBS group due to the inefficient tumor retention of Ce6. For OCZCF treated mice, the slightly suppressed tumor growth indicates the co-effect of GSH depletion and CDT caused by the released Cu ions from OCZCF. After treating with light, OCZCF exhibits significant enhanced tumor inhibition ability. On day 15, the relative tumor volume of mice treated with OCZCF+ is about one third of that in OCZCF group. The difference should be attributed to the synergetic PDT and CDT effect. Notebly, the tumor regression rate of OCZCF+ treated mice is also much higher than that induced by CZCF+. The result suggests the alleviation of tumor hypoxia is of great

significance in enhancing synergistic therapeutic efficiency. Similar tumor suppression behavior are observed in H&E staining of tumor tissues, in which tumors treated with CZCF+ and OCZCF+ exhibit more necrosis slices (**Figure 5d)**. In addition, the evenly increased body weight, histological analyses and hematological indicators of mice in each experiment groups show negligible side effects of OCZCF(**Figure 5b, 5e, Table S6**). Therefore, the oxygen loaded OCZCF could be used as an efficient and biocompatible nanodrug for enhanced synergistic therapy.

2.7. In Vivo biodistribution of OCZCF. In order to determine the in vivo biodistribution of OCZCF, the organs including heart, liver, spleen, lung, kidney and tumors were gathered at intervals after tail vein injection. The zinc levels were ascertained by ICP-MS. **Figure S15** reveals that during the first 12 h after tail vein injection, the OCZCF primarily accumulated in liver and spleen. Because of the EPR effect,[47-49] the cumulative amount of OCZCF reaches the maximum in tumors at around 24 h. Then amount of OCZCF began to decline with the incremental time.

3. CONCLUSIONS

In summary, we successfully fabricated a pH-degradable core/shell-structured nanoplatform, O_2-Cu/ZIF-8@Ce6/ZIF-8@F127 (OCZCF), with TME responses for synergistic photo/chemo-dynamic therapy. The doped Cu^{2+} can double the O_2 loading capacity of ZIF-8, which is in favor of overcoming hypoxic TME and increasing the ROS amount generated by Ce6 under 650 nm laser irradiation. More importantly, the released Cu^{2+} can not only oxidize intratumoral GSH, reducing the unnecessary ROS consumption caused by GSH, but also catalyze the overexpressed H_2O_2 in TME to generate O_2 for further hypoxia alleviation. Noticeably, the byproduct, Cu^{+}, will further induce CDT process by reacting with H_2O_2 to produce cytotoxic •OH via Fenton-like reaction. Both in vitro and in vivo experiments indicate that OCZCF shows better antitumor efficacy through GSH depletion and O_2 replenishment in the combination therapy. This integrated nanoplatform may open up a new way for engeneering high efficient therapeutic reagents for clinical tumor treatment.

4. MATERIALS AND METHODS

4.1. Materials. Methanol, hydrogen peroxide (H_2O_2, 30%) were obtained from Beijing Chemical Regent Co. Ltd. Zinc nitrate hexahydrate (≥98%, $Zn(NO_3)_2$•$6H_2O$), copper nitrate trihydrate (≥98%, $Cu(NO_3)_2$•$3H_2O$), 2-methylimidazole (98%, $C_4H_6N_2$, 2-MI), Pluronic@F127 (F127), 1,3-diphenylisobenzofuran (DPBF), glutathione (GSH), 2,2,6,6-tetramethylpiperidine (TEMP), 5,5-dimethyl-1-pyrroline-N-oxide (DMPO), 3-(4,5-dimethylthiazol-2-yl)-2,5-diphenyltetrazolium bromide (MTT) and 4, 6-diamino-2-phenylindole (DAPI) were purchased from Shanghai Aladdin Bio-Chem Technology Co., Ltd. Chlorin e6 (Ce6) was bought from Shanghai TCI Co., Ltd. Methyl blue (MB) was obtained from Shanghai Sinopharm Co. Ltd. Annexin V-FITC/PI double staining apoptosis detection kit was purchased from Shanghai BestBio. Calcein-AM/PI Double Stain Kit was bought from Beyotime Biotechnology. Reduced Glutathione (GSH) Assay Kit was purchased from Beijing Solarbio Science & Technology Co., Ltd. ROS-ID™ Hypoxia/Oxidative stress detection kit was obtained from Enzo Life Sciences. All chemical reagents were directly used without further purification.

4.2. Instrument and characteristics. Dynamic light scattering (DLS) and surface Zeta potential experiment were tested on a Zetasizer Nano (Malvern). Inductively coupled

plasma (ICP) was obtained from an iCAP 6300 of Thermo scientific. Powder X-ray diffraction (PXRD) patterns were conducted on D8 Focus diffractometer (Bruker) equipped with a Cu-Kα radiation source (λ=1.54182 Å) at 40 kV and 30 mA in the range 5 - 50 degrees. Transmission electron microscope (TEM) was used with a field emission gun operating at 200 kV. EDX analysis of single nanoparticle was measured on the same TEM instrument with attached EDS probe. Scanning electron microscope (SEM) images were obtained from S-4800 (Hitachi) at an acceleration voltage of 10 kV and a working distance of 8 mm. The X-ray photoelectron spectra (XPS) were obtained by ECSALAB 250. UV-Vis spectra were acquired using a U-3310 spectrophotometer. The sorption isotherms for nitrogen and oxygen were measured with an automatic volumetric adsorption apparatus (Micromeritics ASAP 2020 M) at 77 K and 298 K, respectively. Fouriere-transform infrared spectra (FT-IR) were obtained on a Vertex Perkin-Elmer 580BIR spectrophotometer (Bruker). Thermogravimetric analysis (TGA) were measured on Thermal Analysis Instrument (SDT 2960, TA Instruments, New Castle, DE) in a nitrogen flow. The as-synthesized samples (weight 40 - 60 mg) were

dried in air and subsequently dried in desiccator under vacuum. Electron spin resonance (ESR) spectra were obtained from JES-FA200 Spectrometers (JEOL).

4.3. Fabrication of ZIF-8, Cu-doped ZIF-8 (Cu/ZIF-8) and O_2-Cu/ZIF-8@Ce6/ZIF-8@F127 (OCZCF). The ultrasmall ZIF-8 nanoparticles were prepared with the method modified from literature.[50,51] In brief, 2-MI (1.62 g) was mixed with $Zn(NO_3)_2{\cdot}6H_2O$ (733.2 mg) in methanol. After stirring at room temperature for 30 min, the final white products were purified by centrifuging.

Cu/ZIF-8 was prepared as mentioned above except for using the mixture of $Zn(NO_3)_2{\cdot}6H_2O$ and $Cu(NO_3)_2{\cdot}6H_2O$ with desired amount instead of pure $Zn(NO_3)_2{\cdot}6H_2O$ powder. The final products were collected under centrifugation. For the fabrication of O_2-loaded nanocarrier, Cu/ZIF-8 nanoparticles were vacuum dried to eliminate excess methanol in pores. After pumping with O_2 for 3 days, the products were redispersed in methanol for further use. Then, photosensitizer Ce6 loaded ZIF-8 shell was homogeneously grown around O_2-Cu/ZIF-8. Ce6 (2 mg) and Cu/ZIF-8 (20 mg) were first dispersed in 2-MI solution (10 mL, 0.01 M) and then mixed with $Zn(NO_3)_2{\cdot}6H_2O$ solution (10 mL, 0.01 M). The mixture was stirred at room temperature

for 2 h. The dark green products were collected by centrifugation and dissolved in EtOH. Finally, F127 (5 mg) was dissolved in 1 mL of EtOH and mixed with OCZC solution (1mL) for 2 h. The final products were obtained by centrifugation.

4.4. Drug Release Property. To measure the oxygen release behavior, OCZCF (40 mg) was dispersed in deoxygenated PBS solution (20 mL, pH = 6.5 and 7.4). Then the dissolved O_2 amount was read by a portable dissolved oxygen meter. The released Ce6 was analyzed using UV–Vis spectrometer. OCZCF were dispersed in PBS solution (pH = 6.5 and 7.3). Then, the supernatant was taken out at pre-determined time points and dilute with EtOH. The absorbance of Ce6 at 410 nm was measured, based on a standard curve of free Ce6. ICP was used to characterize copper ions released from OCZCF. OCZCF were dispersed in PBS solution (pH = 6.5 and 7.3). The supernatant were diluted by 10 times before test.

4.5. ROS Generation. Singlet oxygen ($^1O_2$) generated by Ce6 under light irradiation (650 nm, 50 mW cm^{-1}) was measured with DPBF probe.[66] DPBF solution (pH = 6.5 and 7.3) was added with CZCF or OCZCF, respectively. Next, UV-Vis spectrometer was used for DPBF analysis. The generation of extracellular hydroxyl radicals (•OH) was

measured with MB.[67] All materials were mixed in PBS buffer (pH = 6.5) containing MB (0.01 μg mL^{-1}). For ESR measurements, 100 μL of aqueous solution of samples (1 mg/L) was mixed with 500 μL of TEMP (50 mM) solution. After being irradiated upon 650 nm laser for 5 min, the mixture was characterized using a Bruker EMX plus model spectrometer operating at the X-band frequency at room temperature. The •OH detection was also performed as described above, except the irradiation and the use of DMPO (50 mM) as the spin-trapping agent.

4.6. GSH Depletion and O_2 Generated by Fenton-Like Reaction. GSH depletion process was tested using reduced glutathione assay kit. In brief, GSH solution (0.01 mM, pH = 6.5) was stirred with ZIF-8, Cu/ZIF-8, and OCZCF, respectively. After centrifugation, the supernatant was measured in line with the accessary specification.

The generation of O_2 from H_2O_2 was tested using a portable dissolved oxygen meter. H_2O_2 (0.1 M) and CZCF (100 mg) were mixed in PBS buffer (pH = 6.5). The generated oxygen was read every 20 s. In comparation, the dissolved oxygen in CZCF solution (pH = 6.5) was also collected.

4.7. Intracellular GSH Consumption. 4T1 were seeded in 6-well plates at 1 × 10^5 cells per well in complete DMEM. Then, cells were treated with PBS, ZCF (ZIF-8@Ce6/ZIF-8@F127) or OCZCF for 12 h. For GSH detection, cells were centrifuged and the redispersed in metaphosphoric acid solution before lysis by three-circle of frozen and thaw. The supernatant was measured in line with the accessary specification.

4.8. Intracellular Hypoxia and ROS Detection. 4T1 cells were seeded in 12-well plates at 1 × 10^5 cells per well in complete DMEM (2 mL) at 37 °C overnight. Then, cells were exposed to normoxic environment (21 % oxygen) or hypoxic environment (1% oxygen) with 5% CO_2 for 8 h. After incubation with CZCF or OCZCF at 50 μg mL^{-1} for 4 h, the light treated groups were exposed to 650 nm irradiation at a power density of 50 mW cm^{-2} for 5 min. Then, Cyto-ID® Hypoxia/Oxidative Stress Detection kit were added into each well for cell imaging. After washed with PBS for several times, cells were stained with DAPI and imaged via inverted fluorescence microscopy.

4.9. Cell Viability Assays. 3-(4,5-dimethylthiazol-2)-2,5-diphenyltetrazole bromide (MTT) reagent was used to evaluate the cytotoxicity. L929 and 4T1 cells were seeded in 96-well plates at 1 × 10^4 cells per well and then exposed to normoxic environment (21 %

oxygen) or hypoxic environment (1% oxygen) with 5% CO_2 for 8 h. PBS, Ce6, CZCF and OCZCF was added to each well with different concentration, respectively. After 4 h incubation, the laser irradiation groups were treated with 650 nm laser at a power density of 50 mW cm^{-2} for 5 min. The cells were then incubated at 37 °C for another 20 h before applying the MTT reagent. For the laser free groups, the plates were incubated in the incubator for 24 h after drug treatment. The absorbance was measured on a Bio-Rad 680 microplate reader at 490 nm.

In addition, calcein-AM and propidium iodide were used to stain the live and dead cells. 4T1 cells were seeded in 12-well plates at 1 × 10^5 cells per well and treated with PBS, Ce6, ZCF, CZCF or OCZCF under hypoxia, respectively. The concentration of nanodrug was 20 μg mL^{-1}. The laser irradiation groups were exposed to 650 nm laser at a power density of 50 mW cm^{-2} for 5 min. Then, dye mixture were added into each well and incubated for 30 min in dark condition. After thoroughly washed with PBS, cells were observed under the inverted fluorescence microscopy.

The cell viability after incubation with CZCF or OCZCF was conducted by flow cytometer under hypoxia. 4T1 cells were seeded into 6-well culture plates and

incubated with 20 μg mL^{-1} CZCF or OCZCF, respectively. 4 h later, cells were irradiated by 650 nm laser at a power density of 50 mW cm^{-2} for 5 min. After 8 h incubation, cells were thoroughly washed with trypsinization and PBS and stained by annexin V-FITC and PI staining kit. The cell apoptosis was characterized by FACS Calibur flow cytometer (BD Biosciences).

4.10. In Vivo Tumor-Bearing Mice Experiment. Female Balb/c mice were purchased from the Center of Experimental Animals, Jilin University (Changchun, China). The animal experiments perform under the criterions of The National Regulation of China for Care and Use of Laboratory Animals. 30 mice (about 20 g) were subcutaneously injected with 1×10^6 4T1 cells to obtain tumor-bearing mice and separated into 5 groups (PBS, Ce6 with light irradiation (Ce6+), O_2-Cu/ZIF@Ce6/ZIF-8@F127 (OCZCF), Cu/ZIF@Ce6/ZIF-8@F127 with light irradiation (CZCF+) and O_2-Cu/ZIF@Ce6/ZIF-8@F127 with light irradiation (OCZCF+) treated groups). Each group contained 6 mice and all materials were used with the Ce6 concentrations to be 4.0 mg kg^{-1} body weight. Nanoparticles were injected intravenously on the 1st and 3rd day. 650 nm laser (50 mW cm^{-2}, 10 min) were used during the irradiation treatment after 24 h post injection. The

weight and tumor sizes of all mice were measured every other day. Mice were euthanized after 15 days and the blood were harvested for hematology studies.

4.11. In vivo biodistribution of OCZCF. To determine the biodistribution of OCZCF, after i.v. injection, the tested organs and tumors from mice (n = 3) were gathered at intervals. Then the organs were weighted and dissolved in mixed solution of HCl and HNO_3 (v/v = 3:1) under heating at 60 ^oC for 10 h. Finally, Zn content in different samples was measured by ICP-MS after being diluted with deionized water.

ASSOCIATED CONTENT

SUPPORTING INFORMATION

This material is available free of charge via the Internet at http://pubs.acs.org.

List of Abbreviations; the average diameter and yeild of Cu/ZIF-8; PXRD patterns; polydispersity index and zeta potential measurements; UV-vis absorption spectra; BET adsorption data; XPS spectra; SEM and TEM images; ICP results; ESR spectra; measurement of GSH content; uptake of OCZCF; tumor slices with ROS and HIF-1α

fluorescence staining; flow cytometry analysis; photograph of tumors; blood biochemical indexes; in vivo biodistribution of OCZCF

AUTHOR INFORMATION

Corresponding Author

* zycheng@ciac.ac.cn.

* jlin@ciac.ac.cn.

ACKNOWLEDGMENT

This work is financially supported by Science and Technology Cooperation Project between Chinese and Australian Governments (2017YFE0132300), the National Natural Science Foundation of China (NSFC 51720105015, 51572257, 51828202, 51772288, and 21728101), Chinese Academy of Sciences (YZDY-SSWJSC018), CAS-Croucher Funding Scheme for Joint Laboratories (CAS18204), and the Science and Technology Development Plan of Jilin Province (20170101187JC and 20170414003GH).

ABBREVIATIONS

Cu/ZIF-8 for Cu-doped ZIF-8; CZCF for Cu/ZIF-8@Ce6/ZIF-8@F127 Nanocomposites; OCZC for O_2-Cu/ZIF-8@Ce6/ZIF-8 Nanocomposites; OCZCF for O_2-Cu/ZIF-8@Ce6/ZIF-8@F127 Nanocomposites.

REFERENCES

(1) Siegel, R. L.; Miller, K. D.; Jemal, A., Cancer Statistics, 2017. *Ca-Cancer J. Clin.* **2017,** *67*, 7-30.

(2) Fan, W.; Yung, B.; Huang, P.; Chen, X., Nanotechnology for Multimodal Synergistic Cancer Therapy. *Chem. Rev.* **2017,** *117*, 13566-13638.

(3) Agostinis, P.; Berg, K.; Cengel, K. A.; Foster, T. H.; Girotti, A. W.; Gollnick, S. O.; Hahn, S. M.; Hamblin, M. R.; Juzeniene, A.; Kessel, D., Photodynamic Therapy of Cancer: an Update. *Ca-Cancer J. Clin.* **2011,** *61*, 250-281.

(4) Cheng, L.; Wang, C.; Feng, L.; Yang, K.; Liu, Z., Functional Nanomaterials for Phototherapies of Cancer. *Chem. Rev.* **2014,** *114*, 10869-10939.

(5) Lucky, S. S.; Soo, K. C.; Zhang, Y., Nanoparticles in Photodynamic Therapy. *Chem. Rev.* **2015,** *115*, 1990-2042.

(6) Zhang, C.; Bu, W.; Ni, D.; Zhang, S.; Li, Q.; Yao, Z.; Zhang, J.; Yao, H.; Wang, Z.; Shi, J., Synthesis of Iron Nanometallic Glasses and Their Application in Cancer Therapy by a Localized Fenton Reaction. *Angew. Chem. Int. Ed.* **2016,** *55*, 2101-2106.

(7) Tang, Z.; Liu, Y.; He, M.; Bu, W., Chemodynamic Therapy: Tumour Microenvironment-Mediated Fenton and Fenton-like Reactions. *Angew. Chem. Int. Ed.* **2019,** *58*, 946-956.

(8) Lin, L. S.; Song, J.; Song, L.; Ke, K.; Liu, Y.; Zhou, Z.; Shen, Z.; Li, J.; Yang, Z.; Tang, W., Simultaneous Fenton-like Ion Delivery and Glutathione Depletion by MnO_2-Based Nanoagent to Enhance Chemodynamic Therapy. *Angew. Chem. Int. Ed.* **2018,** *57*, 4902-4906.

(9) Ma, B.; Wang, S.; Liu, F.; Zhang, S.; Duan, J.; Li, Z.; Kong, Y.; Sang, Y.; Liu, H.; Bu, W.; Li, L., Self-Assembled Copper-Amino Acid Nanoparticles for in Situ Glutathione "AND" H_2O_2 Sequentially Triggered Chemodynamic Therapy. *J. Am. Chem. Soc.* **2019,** *141*, 849-857.

(10) Zhou, Z.; Song, J.; Nie, L.; Chen, X., Reactive Oxygen Species Generating Systems Meeting Challenges of Photodynamic Cancer Therapy. *Chem. Soc. Rev.* **2016,** *45*, 6597-6626.

(11) Fan, W.; Huang, P.; Chen, X., Overcoming the Achilles' Heel of Photodynamic Therapy. *Chem. Soc. Rev.* **2016,** *45*, 6488-6519.

(12) Li, X.; Kwon, N.; Guo, T.; Liu, Z.; Yoon, J., Innovative Strategies for Hypoxic-Tumor Photodynamic Therapy. *Angew. Chem. Int. Ed.* **2018**, *57*, 11522-11531.

(13) Pouysségur, J.; Dayan, F.; Mazure, N. M., Hypoxia Signaling in Cancer and Approaches to Enforce Tumor Regression. *Nature* **2006,** *441*, 437-443.

(14) Duan, L.; Yan, X.; Wang, A.; Jia, Y.; Li, J., Highly Loaded Hemoglobin Spheres as Promising Artificial Oxygen Carriers. *ACS Nano* **2012,** *6*, 6897-6904.

(15) Modery-Pawlowski, C. L.; Tian, L. L.; Pan, V.; Sen Gupta, A., Synthetic Approaches to RBC Mimicry and Oxygen Carrier Systems. *Biomacromolecules* **2013,** *14*, 939-948.

(16) Song, X.; Feng, L.; Liang, C.; Yang, K.; Liu, Z., Ultrasound Triggered Tumor Oxygenation with Oxygen-Shuttle Nanoperfluorocarbon to Overcome Hypoxia-Associated Resistance in Cancer Therapies. *Nano Lett.* **2016,** *16*, 6145-6153.

(17) Cheng, Y.; Cheng, H.; Jiang, C.; Qiu, X.; Wang, K.; Huan, W.; Yuan, A.; Wu, J.; Hu, Y., Perfluorocarbon Nanoparticles Enhance Reactive Oxygen Levels and Tumor Growth Inhibition in Photodynamic Therapy. *Nat. Commun.* **2015,** *6*, 8785.

(18) Xie, Z.; Cai, X.; Sun, C.; Liang, S.; Shao, S.; Huang, S.; Cheng, Z.; Pang, M.; Xing, B.; Kheraif, A. A. A.; Lin, J., O_2-Loaded pH-Responsive Multifunctional Nanodrug Carrier for Overcoming Hypoxia and Highly Efficient Chemo-Photodynamic Cancer Therapy. *Chem. Mater.* **2019,** *31*, 483-490.

(19) Gao, S.; Zheng, P.; Li, Z.; Feng, X.; Yan, W.; Chen, S.; Guo, W.; Liu, D.; Yang, X.; Wang, S., Biomimetic O_2-Evolving Metal-organic Framework Nanoplatform for Highly Efficient Photodynamic Therapy Against Hypoxic Tumor. *Biomaterials* **2018**, *178*, 83-94.

(20) Cai, X.; Xie, Z.; Ding, B.; Shao, S.; Liang, S.; Pang, M.; Lin, J., Monodispersed Copper(I)-Based Nano Metal-Organic Framework as a Biodegradable Drug Carrier with Enhanced Photodynamic Therapy Efficacy. *Adv. Sci. 2019*, 1900848.

(21) Cheng, H.; Zhu, J. Y.; Li, S. Y.; Zeng, J. Y.; Lei, Q.; Chen, K. W.; Zhang, C.; Zhang, X. Z., An O_2 Self‐Sufficient Biomimetic Nanoplatform for Highly Specific and Efficient Photodynamic Therapy. *Adv. Funct. Mater.* **2016,** *26*, 7847-7860.

(22) Chen, H.; Tian, J.; He, W.; Guo, Z., H_2O_2-Activatable and O_2-Evolving Nanoparticles for Highly Efficient and Selective Photodynamic Therapy Against Hypoxic Tumor Cells. *J. Am. Chem. Soc.* **2015,** *137*, 1539-1547.

(23) Chen, Q.; Feng, L.; Liu, J.; Zhu, W.; Dong, Z.; Wu, Y.; Liu, Z., Intelligent Albumin–MnO2 Nanoparticles as pH-/H_2O_2-Responsive Dissociable Nanocarriers to Modulate Tumor Hypoxia for Effective Combination Therapy. *Adv. Mater.* **2016,** *28*, 7129-7136.

(24) Fan, W.; Bu, W.; Shen, B.; He, Q.; Cui, Z.; Liu, Y.; Zheng, X.; Zhao, K.; Shi, J., Intelligent MnO_2 Nanosheets Anchored with Upconversion Nanoprobes for Concurrent pH-/H_2O_2-Responsive UCL Imaging and Oxygen-Elevated Synergetic Therapy. *Adv. Mater.* **2015,** *27*, 4155-4161.

(25) Xu, S.; Zhu, X.; Zhang, C.; Huang, W.; Zhou, Y.; Yan, D., Oxygen and Pt(II) Self-Generating Conjugate for Synergistic Photo-Chemo Therapy of Hypoxic Tumor. *Nat. Commun.* **2018,** *9*, 2053.

(26) Zhang, Y.; Wang, F.; Liu, C.; Wang, Z.; Kang, L.; Huang, Y.; Dong, K.; Ren, J.; Qu, X., Nanozyme Decorated Metal-Organic Frameworks for Enhanced Photodynamic Therapy. *ACS nano* **2018,** *12*, 651-661.

(27) Kim, J.; Cho, H. R.; Jeon, H.; Kim, D.; Song, C.; Lee, N.; Choi, S. H.; Hyeon, T., Continuous O_2-Evolving $MnFe_2O_4$ Nanoparticle-Anchored Mesoporous Silica Nanoparticles for Efficient Photodynamic Therapy in Hypoxic Cancer. *J. Am. Chem. Soc.* **2017,** *139*, 10992-10995.

(28) Zheng, D.-W.; Li, B.; Li, C.-X.; Fan, J.-X.; Lei, Q.; Li, C.; Xu, Z.; Zhang, X.-Z., Carbon-Dot-Decorated Carbon Nitride Nanoparticles for Enhanced Photodynamic Therapy against Hypoxic Tumor via Water Splitting. *ACS Nano* **2016,** *10*, 8715-8722.

(29) Mo, R.; Gu, Z., Tumor Microenvironment and Intracellular Signal-activated Nanomaterials for Anticancer Drug Delivery. *Mater. Today* **2016,** *19*, 274-283.

(30) Kuppusamy, P.; Li, H.; Ilangovan, G.; Cardounel, A. J.; Zweier, J. L.; Yamada, K.; Krishna, M. C.; Mitchell, J. B., Noninvasive Imaging of Tumor Redox Status and Its Modification by Tissue Glutathione Levels. *Cancer research* **2002,** *62*, 307-312.

(31) Cramer, S. L.; Saha, A.; Liu, J.; Tadi, S.; Tiziani, S.; Yan, W.; Triplett, K.; Lamb, C.; Alters, S. E.; Rowlinson, S., Systemic Depletion of L-cyst (e) ine with Cyst (e) inase Increases Reactive Oxygen Species and Suppresses Tumor Growth. *Nat. Med.* **2017,** *23*, 120-127.

(32) Fan, H.; Yan, G.; Zhao, Z.; Hu, X.; Zhang, W.; Liu, H.; Fu, X.; Fu, T.; Zhang, X. B.; Tan, W., A Smart Photosensitizer-manganese Dioxide Nanosystem for Enhanced Photodynamic Therapy by Reducing Glutathione Levels in Cancer Cells. *Angew. Chem. Int. Ed.* **2016,** *55*, 5477-5482.

(33) Ju, E.; Dong, K.; Chen, Z.; Liu, Z.; Liu, C.; Huang, Y.; Wang, Z.; Pu, F.; Ren, J.; Qu, X., Copper (II)–Graphitic Carbon Nitride Triggered Synergy: Improved ROS Generation and Reduced Glutathione Levels for Enhanced Photodynamic Therapy. *Angew. Chem. Int. Ed.* **2016,** *55* 11467-11471.

(34) Kamaly, N.; Xiao, Z.; Valencia, P. M.; Radovic-Moreno, A. F.; Farokhzad, O. C., Targeted Polymeric Therapeutic Nanoparticles: Design, Development and Clinical Translation. *Chem. Soc. Rev.* **2012,** *41*, 2971-3010.

(35) Xu, X.; Ho, W.; Zhang, X.; Bertrand, N.; Farokhzad, O., Cancer Nanomedicine: from Targeted Delivery to Combination Therapy. *Trends Mol. Med.* **2015,** *21*, 223-232.

(36) Sharma, P.; Allison, James P., Immune Checkpoint Targeting in Cancer Therapy: Toward Combination Strategies with Curative Potential. *Cell* **2015,** *161*, 205-214.

(37) Furukawa, H.; Cordova, K. E.; O'Keeffe, M.; Yaghi, O. M., The Chemistry and Applications of Metal-Organic Frameworks. *Science* **2013,** *341*, 1230444.

(38) Wu, M. X.; Yang, Y. W., Metal-Organic Framework (MOF)-Based Drug/Cargo Delivery and Cancer Therapy. *Adv. Mater.* **2017,** *29*, 1606134.

(39) He, C.; Liu, D.; Lin, W., Nanomedicine Applications of Hybrid Nanomaterials Built from Metal–Ligand Coordination Bonds: Nanoscale Metal-Organic Frameworks and Nanoscale Coordination Polymers. *Chem. Rev.* **2015,** *115*, 11079-11108.

(40) Horcajada, P.; Gref, R.; Baati, T.; Allan, P. K.; Maurin, G.; Couvreur, P.; Ferey, G.; Morris, R. E.; Serre, C., Metal-organic Frameworks in Biomedicine. *Chem. Rev.* **2011,** *112*, 1232-1268.

(41) DeCoste, J. B.; Weston, M. H.; Fuller, P. E.; Tovar, T. M.; Peterson, G. W.; LeVan, M. D.; Farha, O. K., Metal-Organic Frameworks for Oxygen Storage. *Angew. Chem. Int. Ed.* **2014,** *53*, 14092-14095.

(42) Moghadam, P. Z.; Islamoglu, T.; Goswami, S.; Exley, J.; Fantham, M.; Kaminski, C. F.; Snurr, R. Q.; Farha, O. K.; Fairen-Jimenez, D., Computer-aided Discovery of a Metal-Organic Framework with Superior Oxygen Uptake. *Nat. Commun.* **2018,** *9*, 1378.

(43) Park, K. S.; Ni, Z.; Côté, A. P.; Choi, J. Y.; Huang, R.; Uribe-Romo, F. J.; Chae, H. K.; O'Keeffe, M.; Yaghi, O. M., Exceptional Chemical and Thermal Stability of Zeolitic Imidazolate Frameworks. *Proc. Natl. Acad. Sci. U. S. A.,* **2006,** *103*, 10186-10191.

(44) Zheng, H.; Zhang, Y.; Liu, L.; Wan, W.; Guo, P.; Nyström, A. M.; Zou, X., One-pot Synthesis of Metal-Organic Frameworks with Encapsulated Target Molecules and Their Applications for Controlled Drug Delivery. *J. Am. Chem. Soc.* **2016,** *138*, 962-968.

(45) Li, S.; Wang, K.; Shi, Y.; Cui, Y.; Chen, B.; He, B.; Dai, W.; Zhang, H.; Wang, X.; Zhong, C.; Wu, H.; Yang, Q.; Zhang, Q., Novel Biological Functions of ZIF-NP as A Delivery Vehicle: High Pulmonary Accumulation, Favorable Biocompatibility, and Improved Therapeutic Outcome. *Adv. Funct. Mater.* **2016,** *26*, 2715-2727.

(46) Russell, B.; Villaroel, J.; Sapag, K.; Migone, A. D., O_2 Adsorption on ZIF-8: Temperature Dependence of the Gate-Opening Transition. *J. Phys. Chem. C* **2014,** *118*, 28603-28608.

(47) Cabral, H.; Miyata, K.; Osada, K.; Kataoka, K., Block Copolymer Micelles in Nanomedicine Applications. *Chem. Rev.* **2018,** *118*, 6844-6892.

(48) Fang, J.; Nakamura, H.; Maeda, H., The EPR Effect: Unique Features of Tumor Blood Vessels for Drug Delivery, Factors Involved, and Limitations and Augmentation of the Effect. *Adv. Drug Delivery Rev.* **2011,** *63*, 136-151.

(49) Shi, J.; Kantoff, P. W.; Wooster, R.; Farokhzad, O. C., Cancer Nanomedicine: Progress, Challenges and Opportunities. *Nat. Rev. Cancer* **2016,** *17*, 20-37.

(50) Zareba, J. K.; Nyk, M.; Samoć, M., Co/ZIF-8 Heterometallic Nanoparticles: Control of Nanocrystal Size and Properties by a Mixed-Metal Approach. *Cryst. Growth Des.* **2016,** *16*, 6419-6425.

(51) Schejn, A.; Aboulaich, A.; Balan, L.; Falk, V.; Lalevée, J.; Medjahdi, G.; Aranda, L.; Mozet, K.; Schneider, R., Cu^{2+}-doped Zeolitic Imidazolate Frameworks (ZIF-8): Efficient and Stable Catalysts for Cycloadditions and Condensation Reactions. *Catal. Sci. Technol.* **2015,** *5*, 1829-1839.

(52) de Villota, E. D.; CARMONA, M. G.; Rubio, J.; DE ANDRÉS, S. R., Equality of the in Vivo and in Vitro Oxygen-Binding Capacity of Haemoglobin in Patients with Severe Respiratory Disease. *Br J Anaesth* **1981,** *53*, 1325-1328.

(53) Oxygen Transport by Hemoglobin. In *Comprehensive Physiology*, **2012**, *2*, 1463-1489.

(54) Lee, H. J.; Cho, Y. J.; Cho, W.; Oh, M., Controlled Isotropic or Anisotropic Nanoscale Growth of Coordination Polymers: Formation of Hybrid Coordination Polymer Particles. *ACS Nano* **2012,** *7*, 491-499.

(55) Park, H.; Na, K., Conjugation of The Photosensitizer Chlorin e6 to Pluronic F127 for Enhanced Cellular Internalization for Photodynamic Therapy. *Biomaterials* **2013,** *34*, 6992-7000.

(56) Hu, F.; Mao, D.; Wang, Y.; Wu, W.; Zhao, D.; Kong, D.; Liu, B., Metal-Organic Framework as a Simple and General Inert Nanocarrier for Photosensitizers to Implement Activatable Photodynamic Therapy. *Adv. Funct. Mater.* **2018,** *28*, 1707519.

(57) Zhang, W.; Li, S.; Liu, X.; Yang, C.; Hu, N.; Dou, L.; Zhao, B.; Zhang, Q.; Suo, Y.; Wang, J., Oxygen-Generating MnO_2 Nanodots-Anchored Versatile Nanoplatform for Combined Chemo-Photodynamic Therapy in Hypoxic Cancer. *Adv. Funct. Mater.* **2018,** *28*, 1706375.

(58) Dubale, A. A.; Tamirat, A. G.; Chen, H.-M.; Berhe, T. A.; Pan, C.-J.; Su, W.-N.; Hwang, B.-J., A Highly Stable CuS and CuS-Pt Modified Cu_2O/CuO Heterostructure as an Efficient Photocathode for the Hydrogen Evolution Reaction. *J. Mater. Chem. A* **2016,** *4*, 2205-2216.

(59) Aguilar, T.; Navas, J.; Alcántara, R.; Fernández-Lorenzo, C.; Gallardo, J.; Blanco, G.; Martín-Calleja, J., A Route for the Synthesis of Cu-Doped TiO_2 Nanoparticles with a Very Low Band Gap. *Chem. Phys. Lett.* **2013,** *571*, 49-53.

(60) Hu, Y.; Liu, Z.; Xu, J.; Huang, Y.; Song, Y., Evidence of Pressure Enhanced CO_2 Storage in ZIF-8 Probed by FTIR Spectroscopy. *J. Am. Chem. Soc.* **2013,** *135*, 9287-9290.

(61) Wei, J.; Li, J.; Sun, D.; Li, Q.; Ma, J.; Chen, X.; Zhu, X.; Zheng, N., A Novel Theranostic Nanoplatform Based on Pd@ Pt-PEG-Ce6 for Enhanced Photodynamic Therapy by Modulating Tumor Hypoxia Microenvironment. *Adv. Funct. Mater.* **2018,** *28*, 1706310.

(62) Zhang, W.; Gilstrap, K.; Wu, L.; K. C, R. B.; Moss, M. A.; Wang, Q.; Lu, X.; He, X., Synthesis and Characterization of Thermally Responsive Pluronic F127-Chitosan Nanocapsules for Controlled Release and Intracellular Delivery of Small Molecules. *ACS Nano* **2010,** *4*, 6747-6759.

(63) Huang, P.; Li, Z.; Lin, J.; Yang, D.; Gao, G.; Xu, C.; Bao, L.; Zhang, C.; Wang, K.; Song, H.; Hu, H.; Cui, D., Photosensitizer-Conjugated Magnetic Nanoparticles for In

Vivo Simultaneous Magnetofluorescent Imaging and Targeting Therapy. *Biomaterials* **2011,** *32*, 3447-3458.

(64) Xue, C.; Tu, B.; Zhao, D., Evaporation-Induced Coating and Self-Assembly of Ordered Mesoporous Carbon-Silica Composite Monoliths with Macroporous Architecture on Polyurethane Foams. *Adv. Funct. Mater.* **2008,** *18*, 3914-3921.

(65) Wang, H.; Jiang, S.; Chen, S.; Li, D.; Zhang, X.; Shao, W.; Sun, X.; Xie, J.; Zhao, Z.; Zhang, Q., Enhanced Singlet Oxygen Generation in Oxidized Graphitic Carbon Nitride for Organic Synthesis. *Adv. Mater.* **2016,** *28,* 6940-6945.

(66) Wang, C.; Tao, H.; Cheng, L.; Liu, Z., Near-infrared Light Induced in Vivo Photodynamic Therapy of Cancer Based on Upconversion Nanoparticles. *Biomaterials* **2011,** *32*, 6145-6154.

(67) Ding, B.; Shao, S.; Jiang, F.; Dang, P.; Sun, C.; Huang, S.; Ma, P. a.; Jin, D.; Kheraif, A. A. A.; Lin, J., MnO_2-Disguised Upconversion Hybrid Nanocomposite: An Ideal Architecture for Tumor Microenvironment-Triggered UCL/MR Bioimaging and Enhanced Chemodynamic Therapy. *Chem. Mater.* **2019**, *31*, 2651-2660.

For Table of Contents Use Only:

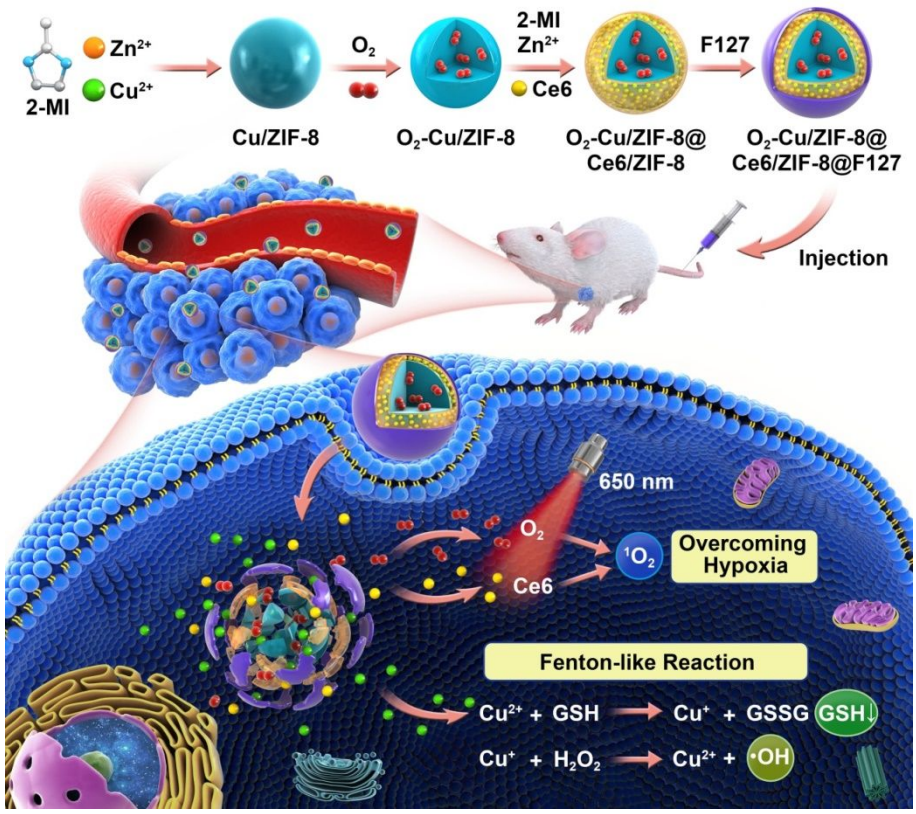
2-MI
Zn2+
Cu2+
Cu/ZIF-8
O2
O2-Cu/ZIF-8
2-MI
Zn2+
Ce6
O2-Cu/ZIF-8@
Ce6/ZIF-8
F127
O2-Cu/ZIF-8@
Ce6/ZIF-8@F127
Injection
650 nm
O2
Ce6
1O2
Overcoming
Hypoxia
Fenton-like Reaction
Cu2+ + GSH → Cu+ + GSSG
GSH↓
Cu+ + H2O2 → Cu2+ + •OH